Hyperpolarized ^{3}He and ^{129}Xe MR Imaging in Healthy Volunteers and Patients with Chronic Obstructive Pulmonary Disease[1]

Miranda Kirby, BSc
Sarah Svenningsen, BMSc
Amir Owrangi, MSc
Andrew Wheatley, BSc
Adam Farag, MSc
Alexei Ouriadov, PhD
Giles E. Santyr, PhD
Roya Etemad-Rezai, MD
Harvey O. Coxson, PhD
David G. McCormack, MD
Grace Parraga, PhD

Purpose: To quantitatively compare hyperpolarized helium 3 (^{3}He) and xenon 129 (^{129}Xe) magnetic resonance (MR) images obtained within 5 minutes in healthy volunteers and patients with chronic obstructive pulmonary disease (COPD) and to evaluate the correlations between ^{3}He and ^{129}Xe MR imaging measurements and those from spirometry and plethysmography.

Materials and Methods: This study was approved by an ethics board and compliant with HIPAA. Written informed consent was obtained from all subjects. Eight healthy volunteers and 10 patients with COPD underwent MR imaging, spirometry, and plethysmography. Ventilation defect percentages (VDPs) at ^{3}He and ^{129}Xe imaging were obtained by using semiautomated segmentation. Apparent diffusion coefficients (ADCs) were calculated from ^{3}He (b = 1.6 sec/cm^2) and ^{129}Xe (b = 12 sec/cm^2) diffusion-weighted images. VDPs at hyperpolarized ^{3}He and ^{129}Xe imaging were compared with a two-tailed Wilcoxon signed rank test and analysis of variance; Pearson correlation coefficients were used to evaluate the relationships among measurements.

Results: ^{129}Xe VDP was significantly greater than ^{3}He VDP for patients with COPD ($P < .0001$) but not for healthy volunteers ($P = .35$), although ^{3}He and ^{129}Xe VDPs showed a significant correlation for all subjects ($r = 0.91$, $P < .0001$). The forced expiratory volume in 1 second (FEV_1) showed a similar and significant correlation with ^{3}He VDP ($r = -0.84$, $P < .0001$) and ^{129}Xe VDP ($r = -0.89$, $P < .0001$), although the correlation between the FEV_1/forced vital capacity (FVC) ratio and ^{129}Xe VDP ($r = -0.95$, $P < .0001$) was significantly greater ($P = .01$) than that for FEV_1/FVC and ^{3}He VDP ($r = -0.84$, $P < .0001$). A significant correlation was also observed for ^{3}He and ^{129}Xe ADC ($r = 0.97$, $P < .0001$); ^{129}Xe ADC was significantly correlated with diffusing capacity of lung for carbon monoxide ($r = -0.79$, $P = .03$) and computed tomographic emphysema measurements (areas with attenuation values in the 15th percentile: $r = -0.91$, $P = .0003$; relative areas with attenuation values of less than −950 HU: $r = 0.87$, $P = .001$).

Conclusion: In patients with COPD, the VDP obtained with hyperpolarized ^{29}Xe MR imaging was significantly greater than that with ^{3}He MR imaging, suggesting incomplete or delayed filling of lung regions that may be related to the different properties of ^{129}Xe gas and physiologic and/or anatomic abnormalities in COPD.

Supplemental material: *http://radiology.rsna.org/lookup/suppl/doi:10.1148/radiol.12120485/-/DC1*

[1] From the Imaging Research Laboratories, Robarts Research Institute, 100 Perth Dr, London, ON, Canada N6A 5K8 (M.K., S.S., A.Owrangi, A.W., A.F., A.Ouriadov, G.E.S., D.G.M., G.P.); Department of Medical Biophysics (M.K., S.S., G.E.S., G.P.), Graduate Program in Biomedical Engineering (A.Owrangi, G.P.), Department of Medical Imaging (R.E.R., G.P.), and Division of Respirology, Department of Medicine (D.G.M.), The University of Western Ontario, London, Ont, Canada; and Department of Radiology & James Hogg Research Centre, St. Paul's Hospital, University of British Columbia, Vancouver, BC, Canada (H.O.C.). Received February 28, 2012; revision requested April 3; revision received April 11; accepted April 11; final version accepted May 8. M.K. is a National Science and Engineering Research Council Scholar and G.P. acknowledges support from a Canadian Institutes of Health Research (CIHR) New Investigator Award. Research funding is gratefully acknowledged from CIHR Operating grants (MOP 97748, MOP 106437) and Team Grant (CIF 97687). **Address correspondence to** G.P. (e-mail: *gparraga@robarts.ca*).

Magnetic resonance (MR) imaging with use of hyperpolarized noble gases such as helium 3 (^{3}He) and xenon 129 (^{129}Xe) provides a way to acquire high spatial and temporal resolution pulmonary images (1–4). Hyperpolarized ^{3}He MR imaging has dominated for the evaluation of gas distribution and tissue abnormalities in healthy volunteers (5); patients with chronic obstructive pulmonary disease (COPD) (6–9), asthma (10–14), cystic fibrosis (15–18), and radiation-induced lung injury (19,20); and lung transplant recipients (21,22). Numerous studies have shown that ^{3}He MR imaging in COPD is highly reproducible (6,23–25), is sensitive to early lung microstructural changes (1,26–31), and shows significant correlation with established measurements of pulmonary function (1,32)—multisection computed tomography (CT) measurements (32) and histologic measurements of emphysema (33). Furthermore, longitudinal ^{3}He MR imaging of COPD has highlighted the sensitivity of the method to progressive worsening (8,34) and shown regional improvements after bronchodilator use (35,36).

Unfortunately, despite the unique potential of ^{3}He MR imaging, clinical translation has not occurred in part because of limited and unpredictable global quantities and high cost. ^{129}Xe gas, conversely, is substantially more abundant in nature, existing in measurable quantities in the atmosphere, and is relatively inexpensive. Although hyperpolarized ^{129}Xe MR imaging is technically challenging because of its nearly threefold lower gyromagnetic ratio and lower enrichment, considerable improvements in ^{129}Xe gas polarization and imaging methods (37) have been achieved since the first clinical studies were reported (38–40). Recently, the tolerability of a 1.0-L inhaled dose of ^{129}Xe and diffusion-weighted MR imaging measurements were reported in patients with COPD and healthy subjects (39,40). These important results suggested that ^{129}Xe MR imaging may be very useful for examining structural and functional abnormalities in COPD and generated numerous hypotheses to test. In this investigation, we hypothesized that the different properties of ^{129}Xe gas would result in significant differences in the ventilation defect percentage (VDP) obtained with ^{129}Xe compared with ^{3}He in patients with COPD but not in healthy volunteers. Accordingly, our objective was to quantitatively compare hyperpolarized ^{3}He and ^{129}Xe MR images obtained within 5 minutes in healthy volunteers and patients with COPD and to evaluate the correlations between ^{3}He and ^{129}Xe MR imaging measurements and those from spirometry and plethysmography.

Advances in Knowledge

- For healthy volunteers and patients with COPD who underwent both helium 3 (^{3}He) and xenon 129 (^{129}Xe) MR imaging within approximately 5 minutes, there were significant and strong correlations between ^{129}Xe and ^{3}He ventilation defect percentages (VDPs) ($r = 0.91$, $P < .0001$); however, for patients with COPD, the VDP with ^{129}Xe MR imaging was significantly greater than that with ^{3}He MR imaging ($P < .0001$).
- There was a similar and strong correlation between VDPs obtained with ^{129}Xe and ^{3}He imaging and forced expiratory volume in 1 second (FEV_1), but the relationship between ^{129}Xe imaging–derived VDP and the FEV_1/forced vital capacity ratio ($r = -.95$, $P < .0001$) was significantly stronger than that for ^{3}He imaging–derived VDP ($P = .01$).
- There were also significant and strong correlations between apparent diffusion coefficients (ADCs) obtained with ^{3}He and those obtained with ^{129}Xe ($r = .97$, $P < .0001$), and both measurements were significantly different in healthy subjects and patients with COPD ($P < .001$).
- In all subjects, ^{129}Xe imaging–derived ADC was significantly correlated with diffusing capacity of lung for carbon monoxide ($r = -.93$, $P < .0001$); for patients with COPD, there were significant correlations with CT measurements of emphysema (areas with attenuation values in the 15th percentile: $r = -.91$, $P = .0003$; relative areas with attenuation values of less than −950 HU: $r = .87$, $P = .001$).

Implication for Patient Care

- Differences between VDPs obtained at ^{129}Xe and ^{3}He MR imaging in COPD may reflect differences in the properties of the gases and physiologic and/or anatomic abnormalities in COPD that are not seen in healthy volunteers.

Materials and Methods

Subjects

All subjects provided written informed consent to the study protocol, which was approved by the local research

Published online before print
10.1148/radiol.12120485 **Content code:** CH

Radiology 2012; 265:600–610

Abbreviations:
ADC = apparent diffusion coefficient
COPD = chronic obstructive pulmonary disease
D_{LCO} = diffusing capacity of lung for carbon monoxide
DW = diffusion weighted
FEV_1 = forced expiratory volume in 1 second
FVC = forced vital capacity
ROI = region of interest
SNR = signal-to-noise ratio
3D = three-dimensional
2D = two-dimensional
VDP = ventilation defect percentage

Author contributions:
Guarantor of integrity of entire study, G.P.; study concepts/study design or data acquisition or data analysis/interpretation, all authors; manuscript drafting or manuscript revision for important intellectual content, all authors; manuscript final version approval, all authors; literature research, M.K., A.F., H.O.C., G.P.; clinical studies, M.K., A.W., A.F., G.E.S., D.G.M.; experimental studies, A.O., G.E.S., R.E.R., G.P.; statistical analysis, M.K., S.S., A.O., A.F., G.P.; and manuscript editing, M.K., S.S., A.O., A.F., A.O., G.E.S., R.E.R., H.O.C., D.G.M., G.P.

Conflicts of interest are listed at the end of this article.

ethics board and Health Canada, and the study was compliant with the Personal Information Protection and Electronic Documents Act of Canada and the Health Insurance Portability and Accountability Act of the United States. Patients with COPD ranged in age from 50 to 85 years and were ex-smokers with a smoking history of at least 10 pack-years. A pack-year was defined as the number of cigarette packs smoked per day multiplied by the number of years smoked. Healthy volunteers were enrolled if they had no history of chronic or current respiratory disease. The mean age of all subjects (±standard deviation) was 71 years ± 8. Men had a mean age of 71 years ± 9, and women had a mean age of 72 years ± 6.

Pulmonary Function Tests

Spirometry was performed by using an EasyOne spirometer (ndd Medizintechnik, Zurich, Switzerland) according to American Thoracic Society guidelines (41). Static lung volumes and diffusing capacity of lung for carbon monoxide (D_{LCO}) were measured by using body plethysmography (MedGraphics, St Paul, Minn).

Image Acquisition

MR imaging was performed with a whole-body 3.0-T unit (Discovery 750MR; GE Healthcare, Milwaukee, Wis) with broadband imaging capability, as previously described (6). Subjects were instructed to inhale a gas mixture from a 1.0-L Tedlar bag (Jensen Inert Products, Coral Springs, Fla) from functional residual capacity, and image acquisition was performed in 8–15 seconds under breath-hold conditions. It is important to note that we endeavored to minimize the potential for differences in the levels of inspiration between the breath-hold images for each subject by *(a)* conducting training and practice sessions for all subjects before MR imaging related to the inspiration breath-hold maneuver from functional residual capacity and *(b)* continuous coaching and monitoring at the MR imaging table by a pulmonary function technologist during all inspiration breath-hold acquisitions.

Conventional hydrogen 1 (^{1}H) MR imaging was performed before hyperpolarized ^{129}Xe and ^{3}He MR imaging, with subjects imaged during 1.0-L breath hold of ultra–high purity medical grade nitrogen 2 (N_2) (Spectra Gases, Alpha, NJ) by using a whole-body radiofrequency coil and a ^{1}H fast spoiled gradient-recalled echo sequence as previously described (6). Theoretical diffusion coefficients for the ^{3}He-N_2 and ^{129}Xe-^{4}He 50/50 mixtures were generated, adopting assumptions previously described (Appendix E1 [online]) (42).

Hyperpolarized ^{3}He MR imaging was enabled by using a linear birdcage transmit-receive chest coil (Rapid Biomedical, Wuerzburg, Germany). A turnkey system (HeliSpin, GE Healthcare) was used to polarize ^{3}He gas to 30%–40%, and doses of 5 mL per kilogram of body weight, diluted with N_2, were administered in 1.0-L Tedlar bags. Hyperpolarized coronal static ventilation ^{3}He MR images and diffusion-weighted (DW) images were acquired during breath hold of a 1.0-L ^{3}He-N_2 mixture as previously described (6).

Hyperpolarized ^{129}Xe MR imaging was enabled by using a custom-made, unshielded quadrature-asymmetric birdcage coil model tuned to 35.34 MHz, similar to previous approaches (43) and as previously described (44). ^{129}Xe gas (86% enriched) was polarized to 10%–60% by using a turnkey polarizer system (XeBox-E10; Xemed, Durham, NH). Doses of hyperpolarized ^{129}Xe gas were dispensed directly into the prerinsed 1.0-L Tedlar bags prefilled with ^{4}He to generate a 50/50 mixture. Polarization of the diluted dose was quantified with use of a Polarimeter (GE Healthcare, Durham, NC). Coronal static ventilation images were acquired by using a three-dimensional (3D) fast gradient-recalled echo sequence with centric phase-encoding ordering in the *y* direction and normal sampling in the *z* direction during breath hold of the 1.0-L ^{129}Xe-^{4}He mixture (data acquisition time = 14 seconds, repetition time msec/echo time msec = 6.7/1.50, variable flip angle, 15.63-kHz bandwidth, 40 × 40-cm field of view, 128 × 128 matrix, 14 sections, 15-mm-thick sections, no gap). DW images were obtained by using a two-dimensional (2D) fast gradient-recalled echo sequence with centric phase-encoding ordering. Two interleaved images (total data acquisition time = 16 seconds, 13.5/10, 9° flip angle, 31.25-kHz bandwidth, 40 × 40-cm field of view, 128 × 80 matrix, seven sections; 30-mm-thick sections, no gap), with and without additional diffusion sensitization with b = 12 sec/cm^2 (maximum gradient amplitude = 2.90 G/cm, gradient rise and fall time = 0.5 msec, gradient separation = 2 msec, gradient duration = 2.0 msec, diffusion time = 5 msec). The diffusion time of 5 msec for ^{129}Xe MR imaging was selected on the basis of the theoretical background for optimal gradient sequence parameters (45) and previous findings demonstrating its sensitivity to alveolar enlargement (46). All imaging was completed within approximately 5 minutes of subjects first lying in the MR unit. In addition, based on the calculations for the theoretical diffusion coefficients for ^{3}He and ^{129}Xe and the diffusion times used, the characteristic diffusion length for ^{3}He (~490 μm) is comparable to that for ^{129}Xe (~460 μm), indicating that similar spatial length scales are being investigated.

Computed tomography (CT) was performed with a 64-section unit (Lightspeed VCT; GE Healthcare, Milwaukee, Wis) by using a detector configuration of 64 × 0.625 mm, 120 kVp, effective tube current of 100 mA, tube rotation time of 500 msec, and pitch of 1.0. A single spiral acquisition of the entire lung was acquired from the apex to the base with subjects in the supine position and with breath holding after inhalation of a 1.0-L Tedlar bag of N_2 from functional residual capacity. Reconstruction of the data was performed by using a section thickness of 1.25 mm with a standard convolution kernel.

Image Analysis

Semiautomated segmentation of ^{3}He and ^{129}Xe MR images was performed, similar to approaches that have been previously described for quantification of lung volumes (47), by using custom software generated with Matlab R2007b (Mathworks, Natick, Mass), as previously described (48). ^{3}He MR

imaging of COPD is typically characterized by heterogeneous signal intensity that reflects gas distribution heterogeneity during inspiration breath-hold imaging. To compare the distribution of both ^{3}He and ^{129}Xe gases within the lung, we segmented the ^{3}He and ^{129}Xe images on the basis of pixel signal intensity. Briefly, ^{3}He and ^{129}Xe static ventilation MR images were segmented by using a k-means approach (49) in which voxel intensity values are classified into five clusters ranging from signal void (cluster 1 or ventilation defect volume) and hypointense signal (cluster 2 or partial volume) to hyperintense signal (cluster 5), therefore generating a gas distribution cluster map. For delineation of the ventilation defect boundaries, a seeded region-growing algorithm (50) was used to segment the ^{1}H MR images of the thoracic cavity for registration to the cluster map and ^{3}He and ^{129}Xe VDPs (7) were generated by using ventilation defect volume normalized to the thoracic cavity volume. ^{3}He and ^{129}Xe non-DW images were also segmented by using the same approach, where non-DW images were segmented by using k-means cluster analysis and registered to the corresponding ^{1}H MR imaging sections to calculate VDP (49). Apparent diffusion coefficient (ADC) analysis was performed as previously described (36). The signal-to-noise ratio (SNR) for all ^{3}He and ^{129}Xe static ventilation and non-DW and DW images was determined by calculating the mean voxel value within a 5×5-cm^2 voxel region of interest (ROI) for four representative ROIs within the lung parenchyma and dividing it by the standard deviation of the voxel values for noise inside four representative ROIs of the same size within the image background, where there was no lung structure. The ROIs within the lung parenchyma and the image background were selected independently for each section, with the exception of DW imaging, where the ROIs were selected independently for each non-DW image section, and the coordinates of the lung ROI were applied to the DW image section. The SNR was determined for each section and then averaged to obtain a single SNR value for each subject. CT measurements were performed by using Matlab R2007b; the relative areas with attenuation values of less than −950 HU and areas with attenuation values in the 15th percentile were generated from the frequency distribution of Hounsfield units.

Statistical Methods

Multivariate analysis of variance and one-way analysis of variance were performed with software (IBM SPSS Statistics 20.0; SPSS, Chicago, Ill). A paired two-tailed t test was used for statistical comparison for normally distributed data, and a two-tailed Wilcoxon signed rank test was used for statistical comparison for nonnormally distributed data for tests between ^{3}He and ^{129}Xe VDP, ADC, and SNR by using software (Prism, version 4.00; GraphPad Software, San Diego, Calif). Normality was determined with a Shapiro-Wilk test by using IBM SPSS Statistics 20.0. Two-way mixed-effects repeated measures analysis of variance was used to determine the interactions for VDP measured at both ^{3}He and ^{129}Xe MR imaging and imaging section by using IBM SPSS Statistics 20.0. The agreement between VDP measurements obtained at ^{3}He and ^{129}Xe imaging was evaluated with Bland-Altman plots (51) generated by GraphPad software (Prism, version 4.00). Linear regression (r^2 values) and Pearson correlation coefficients (r values) were used to determine the relationships between imaging and other measurements by using software (Prism, version 4.00). Correlation coefficients were compared (52) by calculating the Fisher z' transformation for each r value, as follows:

$$z' = \frac{1}{2}[\log(1+r) - \log(1-r)],$$

where r is the correlation coefficient for ^{3}He or ^{29}Xe MR imaging (r_{He} and r_{Xe}, respectively). The Z value was then calculated as follows:

$$Z = \frac{z_{He} - z_{Xe}}{\sqrt{\frac{1}{n-3}}},$$

where Z_{He} is the z' of r_{He}, Z_{Xe} the z' of r_{Xe}, and n the number of subjects compared. A Holm-Bonferroni correction (53) was used for multiple paired t tests and all correlations. The Holm-Bonferroni–adjusted P values were determined by ordering P values from smallest to largest, with the smallest P value multiplied by k, where k is the number of hypotheses to be tested. If the resulting modified P value was less than α (type I error rate), the hypothesis was rejected. The next smallest P value was then multiplied by $k - 1$ and the new modified P value compared with α. This process was repeated until the modified P value could not be rejected. In all statistical analyses, results were considered significant when the probability of making a type I error was less than 5% ($P < .05$).

Results

All imaging procedures and maneuvers were well tolerated, and no serious or severe adverse events were reported. There was a single adverse event reported by one patient with COPD (headache 7 hours after completion of MR imaging that resolved without treatment), and this was judged to be unrelated to ^{3}He or ^{129}Xe gas inhalation; the details of the safety and tolerability of ^{129}Xe MR imaging for this study are reported elsewhere (54), and the tolerability of a 1.0-L ^{129}Xe dose (vs the 50/50 mixture used herein) was previously reported (40). Table 1 shows demographic characteristics and pulmonary function measurements for the eight healthy volunteers and 10 patients with COPD. One patient had Global Initiative for Chronic Obstructive Lung Disease (GOLD) class I, six patients had GOLD class II, two patients had GOLD class III, and one patient had GOLD class IV (55). The two subject groups were significantly different with respect to FEV_1, FEV_1/FVC ratio, reserve volume, ratio of reserve volume to total lung capacity, inspiratory capacity, functional residual capacity, and D_{LCO}; there were no significant differences between the groups with respect to age, sex, or body mass index.

Figure 1 shows coronal ^{3}He and ^{129}Xe MR images for the two central sections, where the trachea and two main bronchi are clearly visible, with ^{3}He gas distribution displayed in red and ^{129}Xe gas distribution displayed in purple. The ^{3}He and ^{129}Xe MR images are registered to the gray-scale ^{1}H MR images of the thorax for three representative healthy volunteers and three patients with COPD. For patients with COPD, regions of signal void are observed on ^{129}Xe MR images but are not qualitatively apparent on ^{3}He MR images; these regions are readily observed in the right mid-apical region in one volunteer and in the right and left apical regions in the other two volunteers.

Figure 2 shows the strong and statistically significant correlations between whole-lung ^{3}He and ^{129}Xe VDP (r = 0.91, $P < .0001$) and ^{3}He and ^{129}Xe ADC (r = 0.97, $P < .0001$). Although VDPs at ^{3}He and ^{129}Xe imaging showed significant correlation, Bland-Altman analysis indicates that there was a 9% ± 8 bias (95% limit of agreement: −25% to 7%) for higher VDP for ^{129}Xe MR imaging. Table 2 shows mean gas distribution and ADC measurements for ^{3}He and ^{129}Xe MR imaging. The VDP obtained with ^{129}Xe imaging was significantly greater than that with ^{3}He imaging for the patients with COPD (P = .0003, uncorrected; P = .03, Holm-Bonferroni corrected), and ^{129}Xe signal intensity cluster 3 was significantly different (P = .002, uncorrected; P = .002, Holm-Bonferroni corrected). For healthy volunteers, there was no significant difference between ^{129}Xe VDP and ^{3}He VDP (P = .56); however, there was a significant difference in cluster 4 (P = .008, uncorrected). With Holm-Bonferroni correction, however, this difference was no longer significant (P = .06). For both groups, there was no relationship between the difference in ^{3}He and ^{129}Xe VDPs and image section (P = .99), indicating no bias for differences between ^{3}He and ^{129}Xe VDP for any specific image section. To better understand the potential effect of any difference in pulse sequence parameters for ^{129}Xe (3D acquisition) and ^{3}He (2D acquisition) MR imaging gas distribution measurements, we compared ^{3}He and ^{129}Xe VDPs measured from non-DW images acquired with 2D fast gradient-recalled echo sequences. No significant difference was observed between ^{129}Xe VDPs obtained with 3D acquisition and those measured from non-DW images for the healthy volunteers and patients with COPD (P = .87). ^{3}He VDPs obtained with 2D acquisition were not significantly different from those measured from non-DW images for healthy volunteers (P = .50); however, they were significantly different for patients with COPD (P = .002). This result is in agreement with the 2D ^{3}He and 3D ^{129}Xe MR imaging results that showed there was no difference between ^{3}He and ^{129}Xe VDPs for healthy volunteers but that ^{129}Xe VDP was significantly greater than ^{3}He VDP for patients with COPD. Mean SNR was significantly lower for ^{129}Xe MR imaging (33 ± 17) than for ^{3}He MR imaging (56 ± 25) ($P < .0001$); however, importantly, there was no significant correlation for the difference between ^{3}He and ^{129}Xe SNR and the difference between ^{3}He and ^{129}Xe VDP (r = 0.26, P = .30).

As shown in Table 2, whole lung hyperpolarized ^{3}He and ^{129}Xe ADC was significantly different for the healthy volunteers (P = .002) and the patients with COPD ($P < .0001$). The mean SNRs were 36 ± 16 and 64 ± 29 for DW and non-DW ^{3}He MR imaging, respectively, and 11 ± 6 and 28 ± 19 for DW and non-DW ^{129}Xe MR imaging.

Table 3 shows Pearson correlations between ^{3}He and ^{129}Xe VDP and ADC and pulmonary function measurements. There were significant and similar correlations for ^{3}He and ^{129}Xe MR imaging VDP with FEV_1, although the relationship between VDP and FEV_1/FVC was significantly stronger for ^{129}Xe MR imaging (P = .01). There were also significant and similar correlations for ^{3}He and ^{129}Xe MR imaging ADC and D_{LCO} (Table 3). Figure 3 shows the significant and strong relationships for ^{3}He and ^{129}Xe ADC with relative areas with attenuation values of less than −950 HU (r = 0.90, P = .0005) and areas with

Table 1

Summary of Demographics

Parameter*	Healthy Volunteers (n = 8)	Patients with COPD (n = 10)	P Value†
Mean age (y)	67 (10)	74 (4)	.10
Men	63 (11)	75 (4)	
Women	71 (7)	73 (6)	
No. of men	4	8	.32
BMI (kg/m^2)	25.9 (2.2)	25.4 (5.0)	.79
Pack-years	0 (0)	62 (15)	NA
FEV_1‡	107 (13)	57 (24)	<.001
FVC‡	106 (13)	91 (19)	.08
FEV_1/FVC	0.75 (0.04)	0.46 (0.14)	<.0001
TLC‡	106 (11)	115 (8)	.09
RV‡	105 (19)	159 (46)	.007
RV/TLC‡	0.39 (0.10)	0.53 (0.14)	.03
IC‡	120 (25)	85 (31)	.02
FRC‡	95 (13)	141 (35)	.002
D_{LCO}‡	103 (13)	41 (17)§	<.0001

Note.—Numbers in parentheses are standard deviations.

* BMI = body mass index, FRC = functional residual capacity, IC = inspiratory capacity, RV = reserve volume, TLC = total lung capacity.

† Significant difference between groups ($P < .05$) was determined by using multivariate analysis of variance. The Fisher exact test was performed for categorical variables. NA = not applicable.

‡ Data are percentage predicted values.

§ Available for seven patients.

Figure 1

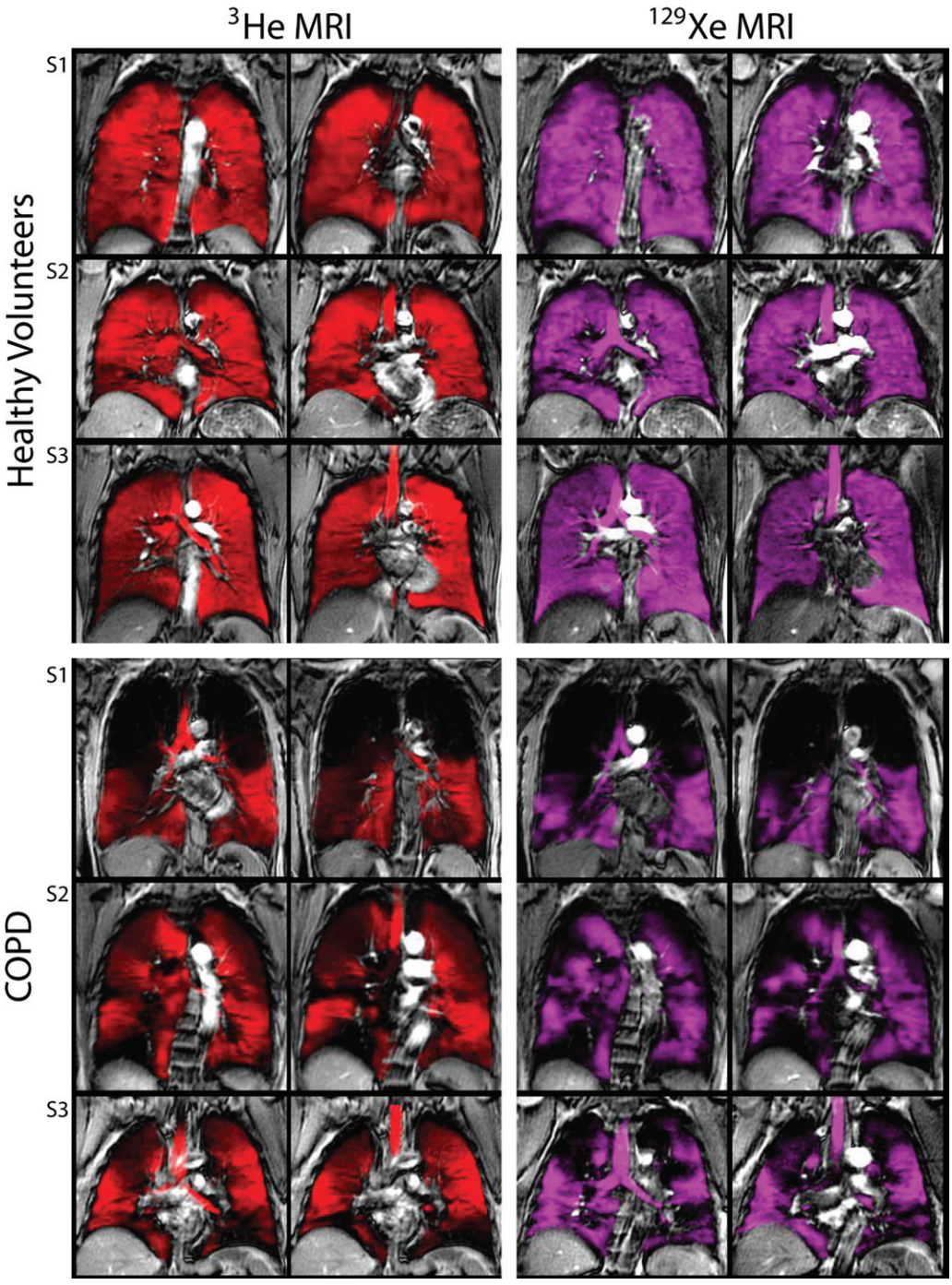

Figure 1: Static ventilation ^{3}He and ^{129}Xe MR images in three healthy volunteers and three patients with COPD. Images of the two coronal center sections, where trachea and two main bronchi are clearly visible, are registered to grayscale ^{1}H MR images of thorax. Volunteer in *S1* is 75-year-old woman with percentage predicted FEV_1 of 93% and FEV_1/FVC of 70%; volunteer in *S2* is 57-year-old man with percentage predicted FEV_1 of 95% and FEV_1/FVC of 72%; volunteer in *S3* is 51-year-old man with percentage predicted FEV_1 of 120% and FEV_1/FVC of 83%. Patient in *S1* is 77-year-old woman with percentage predicted FEV_1 of 50% and FEV_1/FVC of 20%; patient in *S2* is 68-year-old woman with percentage predicted FEV_1 of 59% and FEV_1/FVC of 53%; patient in *S3* is 71-year-old man with percentage predicted FEV_1 of 107% and FEV_1/FVC of 58%. ^{3}He gas distribution is displayed in red and ^{129}Xe gas distribution is displayed in purple.

Table 2

^{3}He and ^{129}Xe MR Imaging Measurements

Parameter	Healthy Volunteers (n = 8)			Patients with COPD (n = 10)		
	^{3}He MR Imaging*	^{129}Xe MR Imaging*	P Value†	^{3}He MR Imaging*	^{129}Xe MR Imaging*	P Value†
Gas distribution (%)						
VDP	4 (2)	4 (4)	.56 (.99)	20 (10)	34 (13)	.003 (.03)
Cluster 2	10 (1)	11 (5)	.94 (.94)	14 (2)	15 (3)	.30 (.99)
Cluster 3	36 (5)	26 (10)	.08 (.48)	34 (5)	22 (6)	.002 (.002)
Cluster 4	34 (2)	40 (2)	.008 (.06)	23 (7)	20 (9)	.05 (.35)
Cluster 5	16 (5)	19 (3)	.22 (.99)	10 (4)	9 (4)	.50 (.99)
ADC (cm^2/sec)	0.246 (.021)	0.053 (.002) ‡	.002 (.02)	0.481 (.121)	0.079 (.015)	<.0001 (.001)

* Numbers in parentheses are standard deviations.

† Significant difference between groups ($P < .05$) was determined by using a two-tailed Wilcoxon signed rank test for gas distribution measurements and a two-tailed paired t test for ADC measurements. Numbers in parentheses are Holm-Bonferroni–adjusted P values.

‡ Available for three subjects.

Figure 2

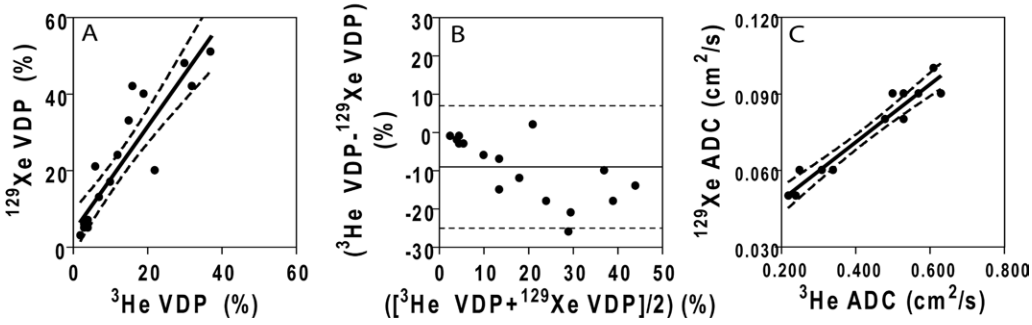

Figure 2: Graphs show relationship between VDP and ADC obtained at ^{3}He and ^{129}Xe MR imaging. *A*, ^{3}He VDP shows significant and positive correlation with ^{129}Xe VDP (r = 0.91, $P < .0001$; r^2 = 0.82, $P < .0001$; $y = 1.4 \times +2.7$). Dashed lines = 95% confidence intervals of regression line. *B*, Mean bias (±standard deviation) between ^{3}He and ^{129}Xe VDP is −9% ± 8 (lower limit = −25%, upper limit = 7%). Solid line = mean difference, dashed lines = 95% limits of agreement. *C*, ^{3}He ADC shows significant and positive correlation with ^{129}Xe ADC (r = 0.97, $P < .0001$; r^2 = 0.93, $P < .0001$; $y = 0.11 \times +0.03$). Dashed lines = 95% confidence intervals of regression line.

attenuation values in the 15th percentile (r = −0.91, P = .0003) for patients with COPD only.

Theoretical diffusion coefficients were generated as previously described (42) for ^{3}He-N_2 and ^{129}Xe-^{4}He and are summarized in Table E1 (online). The ^{3}He-N_2 diffusion coefficient in air for ^{3}He-N_2 was 0.826 cm^2/sec, whereas the diffusion coefficient in air for ^{129}Xe-^{4}He was 0.211 cm^2/sec and the self-diffusion coefficient of air was 0.218 cm^2/sec.

Discussion

We evaluated ^{3}He and ^{129}Xe MR images acquired within approximately 5 minutes in healthy subjects and in patients with COPD and made the following observations: *(a)* significant and strong correlations were observed between VDPs obtained at ^{3}He and ^{129}Xe MR imaging, although visually and quantitatively VDPs obtained with ^{129}Xe MR imaging were worse than those obtained with ^{3}He MR imaging in patients with COPD but not in healthy subjects; *(b)* significant and strong correlations were observed that were similar for ^{3}He and ^{129}Xe VDPs with FEV_1 but significantly stronger between ^{129}Xe VDP and FEV_1/FVC; and *(c)* a significant and strong correlation was observed between ADCs obtained with ^{3}He and ^{129}Xe, both of which showed similar and significant correlations with D_{LCO} and CT measurements of emphysema.

First, in patients with COPD, the gas distribution at ^{129}Xe MR imaging was qualitatively more regionally heterogeneous than that at ^{3}He MR imaging. This was not the case in healthy volunteers, where ^{129}Xe and ^{3}He MR imaging showed homogeneous gas distribution and very low VDPs that were not significantly different. The visually obvious differences between ^{129}Xe and ^{3}He were also quantitatively different, with ^{129}Xe VDP significantly greater (worse) than ^{3}He VDP in patients with COPD but not in healthy

Table 3

Relationships between ^{3}He and ^{129}Xe MR Imaging Parameters and Pulmonary Function Measurements

Pulmonary Function Measurement	^{3}He MR Imaging		^{129}Xe MR Imaging	
	VDP (%)	ADC (cm^2/sec)	VDP (%)	ADC (cm^2/sec)
FEV_1*	−0.84 (<.0001) [<.0001]	−0.75 (.0007) [.002]	−0.89 (<.0001) [.001]	−0.67 (0.01) [.01]
FEV_1/FVC	−0.84 (<.0001) [.001]†	−0.86 (<.0001) [.001]	−0.95 (.0001) [.001]†	−0.77 (.002) [.004]
D_{LCO}*	−0.83 (.0001) [.001]‡	−0.95 (<.0001) [.001]§	−0.92 (<.0001) [.001]‡	−0.93 (<.0001) [.001]‖

Note.—Data are Pearson correlation coefficients. Numbers in parentheses are *P* values. Numbers in brackets are Holm-Bonferroni–adjusted *P* values. Significant difference ($P < .05$) between ^{3}He and ^{129}Xe MR imaging correlation coefficients for each *r* value was calculated by using the Fisher *z′* transformation.

* Data are percentage predicted values.

† The relationship between VDP and FEV_1/FVC was significantly stronger for ^{129}Xe imaging ($P = .01$).

‡ Available for 15 subjects.

§ Available for 13 subjects.

‖ Available for 10 subjects.

Figure 3

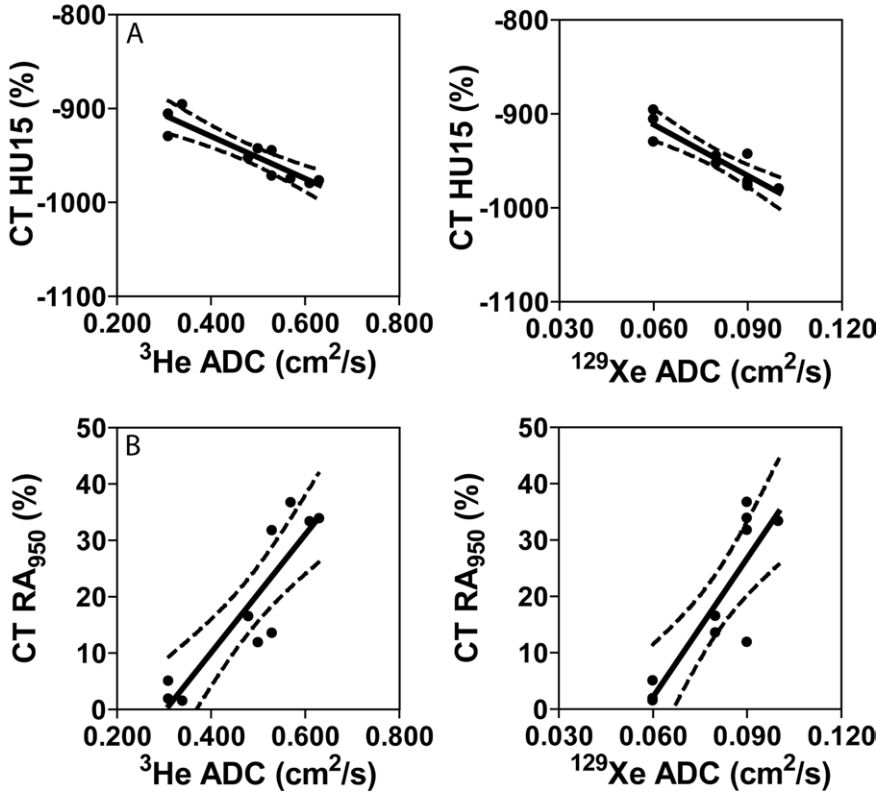

Figure 3: Graphs show relationships between ADCs obtained with ^{3}He and ^{129}Xe MR imaging and CT measurements. *A*, Areas with attenuation values in the 15th percentile *(HU15)* at CT show significant correlation with ^{3}He ADC ($r = -0.91$, $P = .0003$; $r^2 = 0.83$, $P = .0003$; $y = -225 \times -839$) and ^{129}Xe ADC ($r = -0.91$, $P = .0003$; $r^2 = 0.82$, $P = .0003$; $y = -1815 \times -803$). *B*, Relative areas with attenuation values of less than −950 HU at CT *(RA_{950})* show significant correlation with ^{3}He ADC ($r = 0.90$, $P = .0005$; $r^2 = 0.80$, $P = .0005$; $y = 105 \times -32$) and ^{129}Xe ADC ($r = 0.87$, $P = .001$; $r^2 = 0.76$, $P = .001$; $y = 821 \times -47$). Dashed lines = 95% confidence intervals of regression line.

volunteers. Importantly, these differences could not be attributed to differences in the pulse sequences used, nor was there a bias detected for specific anterior-posterior sections dominating this result. This unexpected result leads to the simple question: Why are these measurements different in COPD? Some explanations might derive from the different gases themselves. In COPD, significant airflow limitation is thought to occur in small conducting airways less than 2 mm in diameter (56), increasing airway resistance with the potential for regional and preferential ^{129}Xe gas limitation to the distal airways. Another important consideration relates to the terminal and respiratory bronchioles, where diffusion dominates, and the lower diffusion coefficient of ^{129}Xe relative to ^{3}He may result in slower gas movement into the distal diseased lung regions. Another important consideration is the role of collateral ventilation in COPD. The lower atomic mass and higher diffusivity of ^{3}He relative to ^{129}Xe may allow for regions of lung that are not ventilated to gradually fill with ^{3}He over the time course of breath-hold imaging, as has been shown recently by Marshall et al (57). Our finding that VDP was greater for ^{129}Xe MR imaging than for ^{3}He MR imaging, with both 3D and 2D image acquisition, suggests that the lower diffusivity of ^{129}Xe may slow the process of delayed and/or collateral ventilation

beyond a realistic single-breath-hold time. To try to better understand the properties of the two gases inhaled, we generated theoretical diffusion coefficients as previously described (42) for ^{3}He diluted with N_2 and air and ^{129}Xe diluted with ^{4}He and air and compared these to the theoretical self-diffusion coefficient of air. Taken together, these results indicated that air has a similar estimated diffusion coefficient as ^{129}Xe diluted with ^{4}He and air (within 3%) and that both diffusion coefficients are much lower than the estimated diffusion coefficient of ^{3}He diluted with N_2 and air. Although the exact etiology that may explain the differences between the gas distributions at ^{129}Xe and ^{3}He MR imaging in COPD has not yet been established, it is possible that the differences in diffusion coefficients might provide part of the reason for these observed differences and that different gas mixtures may be helpful in probing different airway and parenchymal abnormalities. For example, the larger ^{129}Xe VDP in COPD might reflect the fact that airway narrowing is less easily penetrated by ^{129}Xe-^{4}He.

Second, we reported significant and similar correlations between ^{3}He and ^{129}Xe VDP and spirometric measurements for all subjects; however, the correlation coefficient was significantly stronger between ^{129}Xe VDP and FEV_1/FVC. We note that, during expiration in COPD, airway narrowing is caused by a combination of many factors, including small-airway wall thickening and obliteration and collapse of airways secondary to the loss of lung tissue within the lungs. FEV_1/FVC is reduced in subjects with severe COPD and asthma and has been reported to be sensitive to airway narrowing and bronchoconstriction (58). The finding that the correlation of VDP with FEV_1/FVC was stronger with ^{129}Xe than with ^{3}He lends support to the notion that the differences in the diffusion coefficients of the gases might be helpful in probing different airway and parenchymal abnormalities.

Finally, we also reported strong and significant correlations between ^{3}He and ^{129}Xe ADCs in the same subjects and similar correlation coefficients between ^{3}He and ^{129}Xe ADCs and D_{LCO} and CT measurements. The relationship between ^{129}Xe ADC and spirometric measurements for $b = 12$ sec/cm^2 has been previously reported (39) in patients with COPD and healthy volunteers, and similar correlation coefficients for the percentage predicted FEV_1 and FEV_1/FVC were observed herein. However, we reported slightly higher ADCs for both healthy volunteers and ex-smokers with COPD, and this may be due to the differences in the inspired gas mixtures between the two different studies. We note that a 1.0-L ^{129}Xe dose was used in the previously published study and, as shown in Table E1 (online), the estimated diffusion coefficient of ^{129}Xe in air was 0.138 cm^2/sec whereas that of ^{129}Xe diluted with ^{4}H and air as used in this study was 0.211 cm^2/sec. In addition, the strong correlations between ^{129}Xe with ^{3}He ADC and the strong and similar correlations between both ^{129}Xe and ^{3}He ADC with CT measurements of emphysema suggest that ^{129}Xe DW imaging with $b = 12$ sec/cm^2 is sensitive to lung microstructural abnormalities. The comparable results we observed with ^{3}He and ^{129}Xe ADCs suggest that both methods are probing similar spatial dimensions, which is important because the choice of DW gradient can influence the measured ADC. We must also note that the patients with COPD investigated herein showed varying degrees of emphysema, with percentage predicted D_{LCO} values ranging from 17% to 67%, indicating that ^{129}Xe MR imaging as used in this study provided a way to measure varying degrees of emphysema. Future studies comparing ^{129}Xe ADC with different b values to ^{3}He ADC and CT emphysema measurements, as well as comparing the ^{129}Xe ADC anterior-posterior gradients with different b values, which has been previously shown by using ^{3}He MR imaging to change following treatment in COPD (36), are required to determine the differences that DW provides for probing the lung microstructure.

We recognize that this work was limited by the small number of subjects and the fact that the analysis was restricted mainly to patients with moderate-to-severe COPD. Therefore, caution should be exercised in extrapolating these results to the general COPD population and, more specifically, patients with mild and very severe disease. We must also acknowledge that because all of these measurements and tests were performed in the same small subject group, extrapolation of these results to a general COPD population cannot be confirmed until studies with larger sample sizes are performed. Another limitation is the difference in pulse sequences used for ^{3}He and ^{129}Xe MR imaging. However, results obtained with non-DW images acquired with 2D fast gradient-recalled echo sequences were in agreement with those from 2D ^{3}He and 3D ^{129}Xe MR imaging, indicating that there was no difference between ^{3}He and ^{129}Xe VDPs for the healthy volunteers. For patients with COPD, however, ^{129}Xe VDP was greater than ^{3}He VDP.

In summary, there was a strong correlation between ^{129}Xe and ^{3}He ADCs in healthy volunteers and patients with COPD but significant differences in ^{129}Xe and ^{3}He gas distribution in COPD, reflecting differences in the gases as well as physiologic and/or anatomic abnormalities in COPD not seen in healthy volunteers.

Acknowledgments: We thank Shayna McKay, BSc, and Sandra Halko, CCRC, RPT, for clinical coordination and clinical database management and Trevor Szekeres, RTMR, for MR imaging of research volunteers. We paid $100 000 annually for the use of an onsite hyperpolarized ^{3}He gas polarizer (Helispin; GE Healthcare, Durham, NC). We also paid $60 000 for 4 weeks use of a ^{129}Xe gas polarizer model XeBox-E10 (Xemed, Durham, NH) during the period September to October 2011.

Disclosures of Conflicts of Interest: M.K. No relevant conflicts of interest to disclose. **S.S.** No relevant conflicts of interest to disclose. **A.Owrangi** No relevant conflicts of interest to disclose. **A.W.** No relevant conflicts of interest to disclose. **A.F.** No relevant conflicts of interest to disclose. **A.Ouriadov** No relevant conflicts of interest to disclose. **G.E.S.** No relevant conflicts of interest to disclose. **R.E.** No relevant conflicts of interest to disclose. **H.O.C.** Financial activities related to the present article: none to disclose. Financial activities not related to the present article: is a paid consultant for Spiration and GSK; institution has grants or grants pending from GSK and Spiration; receives payment for lectures including service on speakers bureaus from As-

traZeneca Australia; receives travel/accommodations/meeting expenses from Spiration, AstraZeneca Australia, and GSK. Other relationships: none to disclose. **D.G.M.** No relevant conflicts of interest to disclose. **G.P.** No relevant conflicts of interest to disclose.

References

1. Salerno M, de Lange EE, Altes TA, Truwit JD, Brookeman JR, Mugler JP III. Emphysema: hyperpolarized helium 3 diffusion MR imaging of the lungs compared with spirometric indexes—initial experience. Radiology 2002;222(1):252–260.
2. Kauczor HU, Ebert M, Kreitner KF, et al. Imaging of the lungs using ^{3}He MRI: preliminary clinical experience in 18 patients with and without lung disease. J Magn Reson Imaging 1997;7(3):538–543.
3. de Lange EE, Mugler JP III, Brookeman JR, et al. Lung air spaces: MR imaging evaluation with hyperpolarized ^{3}He gas. Radiology 1999;210(3):851–857.
4. Möller HE, Chen XJ, Saam B, et al. MRI of the lungs using hyperpolarized noble gases. Magn Reson Med 2002;47(6):1029–1051.
5. Parraga G, Mathew L, Etemad-Rezai R, McCormack DG, Santyr GE. Hyperpolarized ^{3}He magnetic resonance imaging of ventilation defects in healthy elderly volunteers: initial findings at 3.0 Tesla. Acad Radiol 2008;15(6):776–785.
6. Parraga G, Ouriadov A, Evans A, et al. Hyperpolarized ^{3}He ventilation defects and apparent diffusion coefficients in chronic obstructive pulmonary disease: preliminary results at 3.0 Tesla. Invest Radiol 2007;42(6):384–391.
7. Mathew L, Kirby M, Etemad-Rezai R, Wheatley A, McCormack DG, Parraga G. Hyperpolarized ^{3}He magnetic resonance imaging: preliminary evaluation of phenotyping potential in chronic obstructive pulmonary disease. Eur J Radiol 2011;79(1):140–146.
8. Kirby M, Mathew L, Wheatley A, Santyr GE, McCormack DG, Parraga G. Chronic obstructive pulmonary disease: longitudinal hyperpolarized ^{3}He MR imaging. Radiology 2010;256(1):280–289.
9. Choy S, Wheatley A, McCormack DG, Parraga G. Hyperpolarized ^{3}He magnetic resonance imaging–derived pulmonary pressure–volume curves. J Appl Physiol 2010;109(2):574–585.
10. de Lange EE, Altes TA, Patrie JT, et al. Evaluation of asthma with hyperpolarized helium-3 MRI: correlation with clinical severity and spirometry. Chest 2006;130(4):1055–1062.
11. Altes TA, Powers PL, Knight-Scott J, et al. Hyperpolarized ^{3}He MR lung ventilation imaging in asthmatics: preliminary findings. J Magn Reson Imaging 2001;13(3):378–384.
12. Samee S, Altes T, Powers P, et al. Imaging the lungs in asthmatic patients by using hyperpolarized helium-3 magnetic resonance: assessment of response to methacholine and exercise challenge. J Allergy Clin Immunol 2003;111(6):1205–1211.
13. Tzeng YS, Lutchen K, Albert M. The difference in ventilation heterogeneity between asthmatic and healthy subjects quantified using hyperpolarized 3He MRI. J Appl Physiol 2009;106(3):813–822.
14. Fain SB, Gonzalez-Fernandez G, Peterson ET, et al. Evaluation of structure-function relationships in asthma using multidetector CT and hyperpolarized He-3 MRI. Acad Radiol 2008;15(6):753–762.
15. Mentore K, Froh DK, de Lange EE, Brookeman JR, Paget-Brown AO, Altes TA. Hyperpolarized HHe 3 MRI of the lung in cystic fibrosis: assessment at baseline and after bronchodilator and airway clearance treatment. Acad Radiol 2005;12(11):1423–1429.
16. Koumellis P, van Beek EJ, Woodhouse N, et al. Quantitative analysis of regional airways obstruction using dynamic hyperpolarized ^{3}He MRI: preliminary results in children with cystic fibrosis. J Magn Reson Imaging 2005;22(3):420–426.
17. Kirby M, Svenningsen S, Ahmed H, et al. Quantitative evaluation of hyperpolarized helium-3 magnetic resonance imaging of lung function variability in cystic fibrosis. Acad Radiol 2011;18(8):1006–1013.
18. Donnelly LF, MacFall JR, McAdams HP, et al. Cystic fibrosis: combined hyperpolarized ^{3}He-enhanced and conventional proton MR imaging in the lung—preliminary observations. Radiology 1999;212(3):885–889.
19. Mathew L, Gaede S, Wheatley A, Etemad-Rezai R, Rodrigues GB, Parraga G. Detection of longitudinal lung structural and functional changes after diagnosis of radiation-induced lung injury using hyperpolarized ^{3}He magnetic resonance imaging. Med Phys 2010;37(1):22–31.
20. Ireland RH, Bragg CM, McJury M, et al. Feasibility of image registration and intensity-modulated radiotherapy planning with hyperpolarized helium-3 magnetic resonance imaging for non–small-cell lung cancer. Int J Radiat Oncol Biol Phys 2007;68(1):273–281.
21. Zaporozhan J, Ley S, Gast KK, et al. Functional analysis in single-lung transplant recipients: a comparative study of high-resolution CT, ^{3}He-MRI, and pulmonary function tests. Chest 2004;125(1):173–181.
22. McAdams HP, Palmer SM, Donnelly LF, Charles HC, Tapson VF, MacFall JR. Hyperpolarized ^{3}He-enhanced MR imaging of lung transplant recipients: preliminary results. AJR Am J Roentgenol 1999;173(4):955–959.
23. Mathew L, Evans A, Ouriadov A, et al. Hyperpolarized ^{3}He magnetic resonance imaging of chronic obstructive pulmonary disease: reproducibility at 3.0 tesla. Acad Radiol 2008;15(10):1298–1311.
24. Morbach AE, Gast KK, Schmiedeskamp J, et al. Diffusion-weighted MRI of the lung with hyperpolarized helium-3: a study of reproducibility. J Magn Reson Imaging 2005;21(6):765–774.
25. Diaz S, Casselbrant I, Piitulainen E, et al. Hyperpolarized ^{3}He apparent diffusion coefficient MRI of the lung: reproducibility and volume dependency in healthy volunteers and patients with emphysema. J Magn Reson Imaging 2008;27(4):763–770.
26. Evans A, McCormack D, Ouriadov A, Etemad-Rezai R, Santyr G, Parraga G. Anatomical distribution of ^{3}He apparent diffusion coefficients in severe chronic obstructive pulmonary disease. J Magn Reson Imaging 2007;26(6):1537–1547.
27. Yablonskiy DA, Sukstanskii AL, Woods JC, et al. Quantification of lung microstructure with hyperpolarized ^{3}He diffusion MRI. J Appl Physiol 2009;107(4):1258–1265.
28. Yablonskiy DA, Sukstanskii AL, Leawoods JC, et al. Quantitative in vivo assessment of lung microstructure at the alveolar level with hyperpolarized ^{3}He diffusion MRI. Proc Natl Acad Sci U S A 2002;99(5):3111–3116.
29. Saam BT, Yablonskiy DA, Kodibagkar VD, et al. MR imaging of diffusion of (3)He gas in healthy and diseased lungs. Magn Reson Med 2000;44(2):174–179.
30. Fain SB, Panth SR, Evans MD, et al. Early emphysematous changes in asymptomatic smokers: detection with ^{3}He MR imaging. Radiology 2006;239(3):875–883.
31. Fain SB, Altes TA, Panth SR, et al. Detection of age-dependent changes in healthy adult lungs with diffusion-weighted ^{3}He MRI. Acad Radiol 2005;12(11):1385–1393.
32. Diaz S, Casselbrant I, Piitulainen E, et al. Validity of apparent diffusion coefficient hyperpolarized ^{3}He-MRI using MSCT and pulmonary function tests as references. Eur J Radiol 2009;71(2):257–263.

33. Woods JC, Choong CK, Yablonskiy DA, et al. Hyperpolarized ^{3}He diffusion MRI and histology in pulmonary emphysema. Magn Reson Med 2006;56(6):1293–1300.

34. Diaz S, Casselbrant I, Piitulainen E, et al. Progression of emphysema in a 12-month hyperpolarized ^{3}He-MRI study: lacunarity analysis provided a more sensitive measure than standard ADC analysis. Acad Radiol 2009;16(6):700–707.

35. Kirby M, Mathew L, Heydarian M, Etemad-Rezai R, McCormack DG, Parraga G. Chronic obstructive pulmonary disease: quantification of bronchodilator effects by using hyperpolarized ^{3}He MR imaging. Radiology 2011;261(1):283–292.

36. Kirby M, Heydarian M, Wheatley A, McCormack DG, Parraga G. Evaluating bronchodilator effects in chronic obstructive pulmonary disease using diffusion-weighted hyperpolarized helium-3 magnetic resonance imaging. J Appl Physiol 2012;112(4):651–657.

37. Walker TG, Happer W. Spin-exchange optical pumping of noble-gas nuclei. Rev Mod Phys 1997;69(2):629–642.

38. Mugler JP III, Mata JF, Wang HTJ, et al. The apparent diffusion coefficient of 129-Xe in the lung: preliminary human results [abstr]. In: Proceedings of the Twelfth Meeting of the International Society for Magnetic Resonance in Medicine. Berkeley, Calif: International Society for Magnetic Resonance in Medicine, 2004; 769.

39. Kaushik SS, Cleveland ZI, Cofer GP, et al. Diffusion-weighted hyperpolarized ^{129}Xe MRI in healthy volunteers and subjects with chronic obstructive pulmonary disease. Magn Reson Med 2011;65(4):1154–1165.

40. Driehuys B, Martinez-Jimenez S, Cleveland ZI, et al. Chronic obstructive pulmonary disease: safety and tolerability of hyperpolarized ^{129}Xe MR imaging in healthy volunteers and patients. Radiology 2012;262(1):279–289.

41. Miller MR, Hankinson J, Brusasco V, et al. Standardisation of spirometry. Eur Respir J 2005;26(2):319–338.

42. Chen XJ, Möller HE, Chawla MS, et al. Spatially resolved measurements of hyperpolarized gas properties in the lung in vivo. I. Diffusion coefficient. Magn Reson Med 1999;42(4):721–728.

43. De Zanche N, Chhina N, Teh K, Randell C, Pruessmann KP, Wild JM. Asymmetric quadrature split birdcage coil for hyperpolarized ^{3}He lung MRI at 1.5T. Magn Reson Med 2008;60(2):431–438.

44. Farag A, Wang J, Ouriadov A, Parraga G, Santyr G. Unshielded and asymmetric RF transmit coil for hyperpolarized 129Xe human lung imaging at 3.0T [abstr]. In: Proceedings of the Twentieth Meeting of the International Society for Magnetic Resonance in Medicine. Berkeley, Calif: International Society for Magnetic Resonance in Medicine, 2012; 1233.

45. Sukstanskii AL, Yablonskiy DA. Lung morphometry with hyperpolarized 129Xe: theoretical background. Magn Reson Med 2012;67(3):856–866.

46. Boudreau M, Xu X, Santyr GE. Measurement of (129) Xe gas apparent diffusion coefficient anisotropy in an elastase-instilled rat model of emphysema. Magn Reson Med doi:10.1002/mrm.24224. Published online February 29, 2012. Accessed February 29, 2012.

47. Woodhouse N, Wild JM, Paley MN, et al. Combined helium-3/proton magnetic resonance imaging measurement of ventilated lung volumes in smokers compared to never-smokers. J Magn Reson Imaging 2005;21(4):365–369.

48. Kirby M, Heydarian M, Svenningsen S, et al. Hyperpolarized ^{3}He magnetic resonance functional imaging semiautomated segmentation. Acad Radiol 2012;19(2):141–152.

49. MacQueen J. Some methods for classification and analysis of multivariate observations. In: Le Cam LM, Neyman J, eds. Fifth Berkeley Symposium on Mathematical Statistics and Probability; Statistical Laboratory of the University of California, Berkeley. Berkeley, Calif: University of California Press, 1967; 281–297.

50. Adams R, Bischof L. Seeded region growing. IEEE Trans Pattern Anal Mach Intell 1994;16(6):641–647.

51. Bland JM, Altman DG. Statistical methods for assessing agreement between two methods of clinical measurement. Lancet 1986;1(8476):307–310.

52. Comrey AL, Lee HB. Confidence intervals for means and tests on correlations. In: Elementary statistics: a problem solving approach. 4th ed. Morrisville, NC: Lulu, 2009; 103–112.

53. Van Bell G, Fisher L, Heagerty P, Lumley T. Multiple comparisons in biostatistics: a methodology for the health sciences. 2nd ed. Seattle, Wash: Wiley-Interscience, 2004.

54. Shukla Y, Wheatley A, Kirby M, et al. Hyperpolarized (129)Xe magnetic resonance imaging: tolerability in healthy volunteers and subjects with pulmonary disease. Acad Radiol 2012;19(8):941–951.

55. Rabe KF, Hurd S, Anzueto A, et al. Global strategy for the diagnosis, management, and prevention of chronic obstructive pulmonary disease: GOLD executive summary. Am J Respir Crit Care Med 2007;176(6):532–555.

56. Hogg JC, Macklem PT, Thurlbeck WM. The resistance of small airways in normal and diseased human lungs. Aspen Emphysema Conf 1967;10:433–441.

57. Marshall H, Deppe MH, Parra-Robles J, et al. Direct visualisation of collateral ventilation in COPD with hyperpolarised gas MRI. Thorax 2012;67:613–617.

58. Gibbons WJ, Sharma A, Lougheed D, Macklem PT. Detection of excessive bronchoconstriction in asthma. Am J Respir Crit Care Med 1996;153(2):582–589.